25th ABCM International Congress of Mechanical Engineering
October 20-25, 2019, Uberlândia, MG, Brazil

CHARACTERIZATION OF MULTIAXIAL LOW CYCLE FATIGUE PROPERTIES OF SAE 1020 STEEL AND 6351-T6 ALUMINUM ALLOYS

Thiago Almeida Cunha
Jaime Tupiassú Pinho de Castro
Marco Antonio Meggiolaro
Pontifícia Universidade Católica do Rio de Janeiro, Rua Marquês de São Vicente 225, Gávea, Rio de Janeiro, RJ - Brazil - 22451-900
tcunha@ualberta.ca
jtcastro@puc-rio.br
meggi@puc-rio.br

Abstract. *A simplified method to estimate shear (γN) fatigue properties via displacement-controlled experiments is proposed, and used for characterization of SAE 1020 Steel and 6351-T6 Aluminum alloys. This data is compared with the also measured tensile (εN) fatigue properties to identify if these materials are tensile or shear sensitive under multiaxial loading conditions. The Levenberg-Marquardt algorithm is used to optimize the fitting of the experimental data into the Coffin-Manson and in the γN equations, and its implementation procedures are discussed. Finally, the most suitable critical-plane multiaxial fatigue models are proposed for each material tested, based on the measured data.*

Keywords: *low cycle fatigue, multiaxial fatigue, critical plane damage model, Levenberg-Marquardt algorithm*

1. INTRODUCTION

The mechanical failure mechanism known as fatigue is primarily caused by variable loads, which induces cyclic movements of dislocations in the microstructure of the component. In the macroscopic scope, the accumulation of these dislocations initiates and/or propagates a crack. To model this phenomenon and predict the number of cycles necessary for a component to fail, a variety of distinct methodologies are available.

Fatigue failure predictions were first developed by Wöhler in his pioneer work in the mid-nineteenth century (Timoshenko et al). In his SN Method, the ranges and maximum values of cyclic stress are correlated with the number of cycles necessary to initiate a crack. This methodology is recommended for high-cycle fatigue cases, when strains generated by the component constraints are elastic. However, in low-cycle fatigue problems, where plastic deformations are dominant, this method tends to be non-conservative and should not be used (Castro et al.).

The standard methodology for modeling low-cycle fatigue cases is the εN method, which correlates the strain amplitude ε_a and the number of cycles N using the Coffin-Manson rule (Castro et al.), stated by

$$\varepsilon_a = \left(\frac{\sigma_c}{E}\right)(2N)^b + \varepsilon_c(2N)^c \tag{1}$$

where E is Young's modulus, σ_c and ε_c are the elastic and plastic coefficients (also known as fatigue strength and fatigue ductility coefficients) and b and c are their respective exponents. Those constants are calculated based on experimental data, which are commonly obtained following the procedures recommended in the ASTM E606 Standard Test Method for Strain-Controlled Fatigue Testing. Fitting the experimental data generates the εN curve, which assists on the fatigue life prediction of different materials under distinct plastic strain amplitudes.

For pure torsional problems, the Coffin-Manson rule can be adapted into a shear version, known as γN curve, stated by

$$\gamma_a = \left(\frac{\tau_c}{G}\right)(2N)^{b_\gamma} + \gamma_c(2N)^{c_\gamma} \tag{2}$$

where G is the shear modulus of elasticity, τ_c and γ_c are the shear elastic and shear plastic coefficients, and b_γ and c_γ are their respective exponents. Although the γN curve is a direct adaptation of the εN equation, there is no universally accepted model to correlate their coefficients. Different correlations are proposed in the literature. Lagoda et al., for

instance, provides a summary of the most common ones in his work. Thus, experimental data is necessary to evaluate which one is the most suitable for describing the tensile and shear sensitivity of a given material.

In torsional and multiaxial experiments, the influence of the shear stress has to be taken into account in the stress calculation. A methodology that differs from the uniaxial fatigue models is, therefore, necessary. Shear-tensile correlation models enhance the understanding of the material behavior under shear, tensile and combined stresses, and are of great use in the life prediction of real components under multiaxial constraints, as well as material selection and design in new mechanical applications. This article works on the low-cycle fatigue characterization of two metals, the SAE 1020 steel and 6351-T6 aluminum alloy, along with the correlation between their tensile and shear fatigue properties and the identification of the most appropriate critical-plane multiaxial fatigue model. Moreover, in this work a simplified methodology is proposed for torsional experiments to avoid the need to use expensive equipment and different specimen designs.

Each material chosen for the tests has several applications in various engineering designs. As stated on the ASM Metals Handbook, 6xxx series aluminum alloys are commonly used in bicycle frames, transportation equipment, as well as architectural applications because of its good formability, machinability and corrosion resistance. Plain low carbon steels in the 10xx group are used in a variety of applications, because of their relatively inexpensive manufacturing process. Also, both materials are not present on Lagoda et al.'s list of low-cycle fatigue properties, thus data provided in this work serves as an expansion to their research.

This paper is organized as follows. Section II presents the proposed methodology. Section III shows and discusses the experimental results. Finally, Section IV shows the conclusions and suggestions for future work.

2. METHODOLOGY

2.1 Specimen Design

All specimens were designed following the procedures listed on the E606 Standard. A schematic of the specimen is shown in Figure 1, and the measurements used for each material are shown in Table 1.

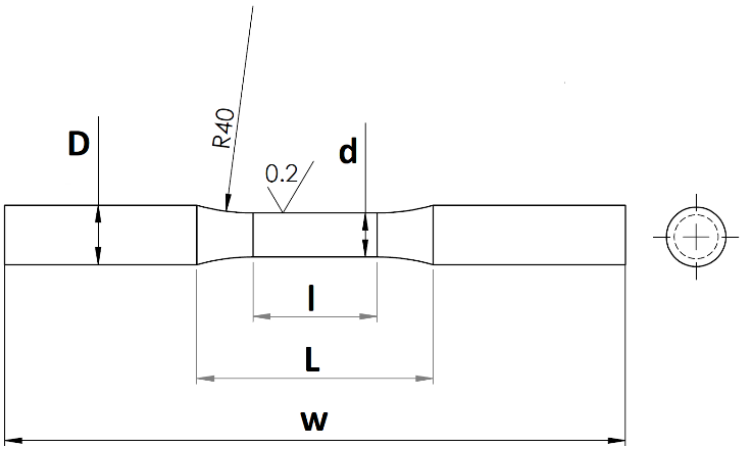

Figure 1. Schematic of the specimen.

Table 1. Specimen measurements (in mm)

Dimensions	SAE 1020 Steel	Aluminum 6351
D	11.8	11.8
d	8.5	10
l	24	18
L	45.7	34.87
w	120	120.8

2.2 Mechanical Properties

For the SAE 1020 steel alloy, the yield strength (S_Y), ultimate strength (S_U) and reduction of the cross-section area of the specimen (AR) were measured following the procedures recommended in the ASTM E8 Standard Methods for Tension Testing of Metallic Materials. Its Young's Modulus was measured calculating the mean of the slope on the elastic part of each experiment. The values measured by Lima et al. for 6351-T6 Aluminum alloy were also used in the present work.

Poisson's ratio (ν) was estimated as ν = 0.29 for steel and ν = 0.32 for aluminum. The shear modulus, yield strain (ε_Y) and ultimate strain (ε_U) were calculated using

$$G = \frac{E}{2(1+\nu)} \tag{3}$$

$$\varepsilon_U = ln\left(\frac{1}{1-AR}\right) \tag{4}$$

$$\varepsilon_Y = \frac{S_Y}{E} \tag{5}$$

2.3 Measuring εN Properties

All tension-compression experimental data was obtained in accordance to the E606 Standard, using the Instron 8501 Servohydraulic Fatigue Testing System, shown in Figure 2. The chosen criteria for determining failure was the Force Drop in 50%, which stated that when the tensile constraint reaches half of its beginning value a crack can be assumed to be present there, reducing the cross-section area of the specimen. An Instron 2630-100 Series Clip-on Extensometer, shown in Figure 2, was chosen to measure the strain amplitudes and to control the servohydraulic machine during the tests.

Figure 2. A) Instron 8501 Servohydraulic Fatigue Testing System; B) Instron 2630-100 Series Clip-on Extensometer; C) Instron 8874 Biaxial Servohydraulic Fatigue Testing System.

2.4 Measuring γN Properties

All torsional experimental data was obtained using the Instron 8874 Biaxial Servohydraulic Fatigue Testing System, shown in Figure 2. As stated in the E2207 Standard for Strain-Controlled Axial-Torsional Fatigue Testing with Thin-Walled Tubular Specimens, the shear stress profile tends to be non-linear for a specimen under elastoplastic

deformations. Tubular specimens are recommended because, depending on their wall thickness, the shear stress gradient can be ignored and the hypothesis of a uniformly distributed shear stress is valid.

Also, strain control demands the use of torsional or biaxial extensometers, an expensive piece of equipment that was not available for this present work. To overcome this problem, a simplified semi-empirical method is proposed here to calculate the shear strain using the angular displacement readings provided by the LVDT of the testing machine.

The proposed methodology is based on the hypothesis that, for uniform geometries (without the presence of notches), the strain profile is still linear even for plastic deformations. This hypothesis is reasonable as long as the cross sections can still be assumed to remain planar. Using the linear strain profile, it is possible to neglect in the analysis the complicated shear stress profile, as shown in Fig. 3. Then, using Eq. (6) from Gere et al., it is possible to relate the measured angular displacement with the shear strain in both elastic and plastic regimes.

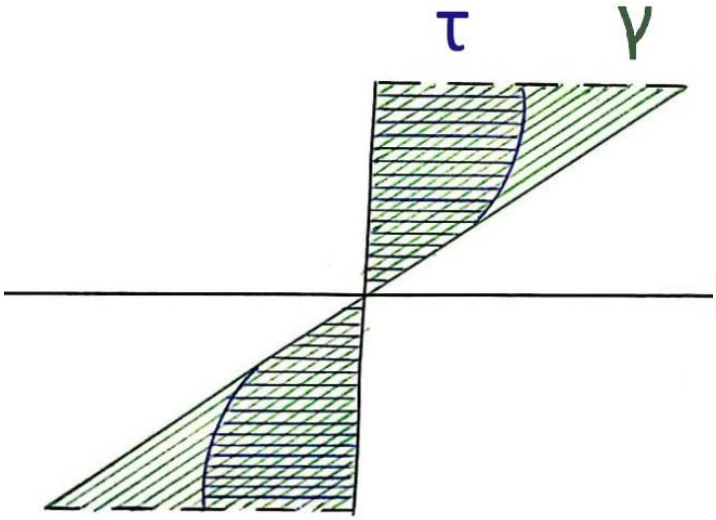

Figure 3. Elastoplastic shear stress and strain profiles on a specimen's cross-section area under pure torsion.

$$\gamma_a = \frac{D}{2L}\left(\varphi_a \frac{\pi}{180}\right) \tag{6}$$

Equation (6) was adapted to receive as input the angle amplitude in degrees, which was the controlling parameter on each torsional experiment, and to calculate the amplitude of the deformation to be used in the γN equation. With the exclusion of the shear stress from the equations, a tubular specimen is not a requirement anymore, and the same specimen design used on the tensile-compression experiments can be used for these experiments. Note however that the shear strain gradient from the solid (instead of hollow) shaft can have a significant effect on the fatigue life, even though it is not modeled in this work.

As recommended in the E606 standard, the specimen has two soft notches. This diameter variation was not considered in Eq. (6), simplifying the model geometry to a uniform solid shaft with the same diameter as the smaller one from the specimen.

The criteria of failure and minimum number of experiments were the same used in the tensile-compression experiments, giving the desired γN curve.

2.5 **Critical Plane Approach**

This subsection is intended for a brief explanation about the Critical Plane approach, its modeling and some of the most commons damage models. For more details about these topics, see Castro et al. Also, in this present work the critical plane is always assumed on a free surface, which is true in all of the experiments conducted.

Extensive experimental evidence shows that, in most metallic alloys and other directional-damage materials, fatigue cracks tend to initiate on specific planes at the critical point, where the damage induced by the loading history is maximized. For this reason, these planes are defined as critical.

To properly represent this behavior, the discussed models assume that stresses on other planes would initiate different fatigue cracks that do not interact, because only the dominant one propagates on the critical plane.

All planes at the critical point are described by their latitudinal (θ) and longitudinal (φ) angles from the surface, as shown in Figure 4. The shear and normal stresses, which corroborate to the crack fatigue initiation, are τ_A, τ_B, and $\sigma_\perp$, and the critical plane only needs to be searched for in the angular ranges $0° < \varphi < 90°$ and $0° < \theta < 180°$, due to plane symmetries.

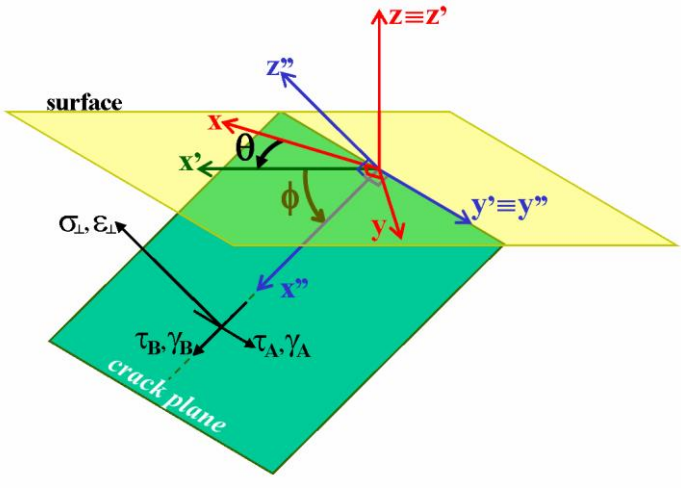

Figure 4. Coordinate transformations, where z is defined perpendicular to the free surface (Castro et al.)

Bannantine and Socie proposed a simplified procedure to search for the critical plane assuming that, for directional-damage materials, the most common microcracks always appear at φ=90º (Case A) or at φ=45º (Case B), shown in Figure 5. They are formed in three different ways and are named:

- A90(T) cracks at φ=90º, caused mainly by the tensile stress (σ⊥) or strain (ε⊥) perpendicular to the plane;
- A90(S) cracks at φ=90º, caused mainly by the in-plane shear stress (τ_A) or strain (γ_A);
- B45(S) cracks at φ=45º, caused mainly by the out-of-plane shear stress (τ_B) or strain (γ_B).

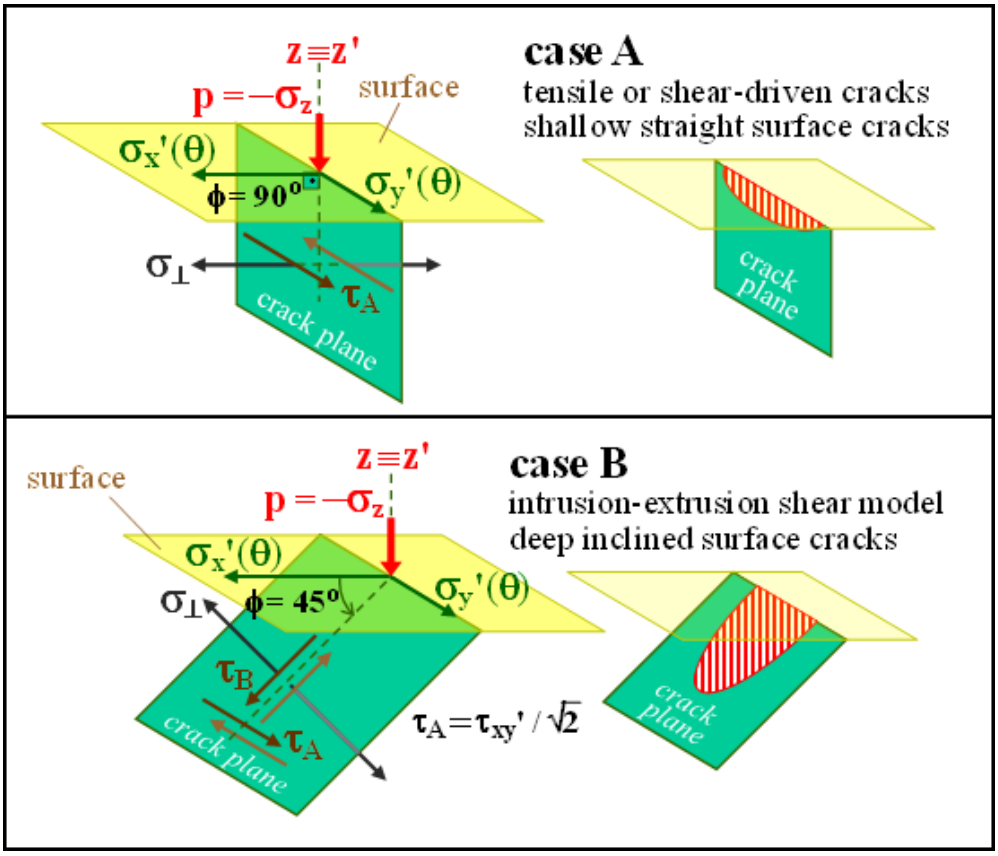

Figure 5. Stress states for the initiation of A90 and B45 cracks (modified from Castro et al.)

This modeling highlights the importance of characterizing the tensile or shear sensitivity of materials to precisely predict their lives under cyclic multiaxial loadings. For that reason, critical plane multiaxial fatigue models assume a different selection of those parameters to be the driven forces on the crack formation, being classified as shear or tensile models. Some of the most common ones are shown next, and their respective formulas are shown in Eqs. (7-10), where

S_{Yc} is the cyclic yield strength (for materials that cyclic harden or soften), $S_F(N)$ is the fatigue strength for an expected number of cycles and α, β are constants of the models.

$$\max_{\theta,\varphi}\left[\frac{\Delta\tau(\theta,\varphi)}{2}+\alpha_F\sigma_{\perp\max}(\theta,\varphi)\right]=\beta_F \tag{7}$$

$$\max_{\theta,\varphi}\left[\frac{\Delta\gamma(\theta,\varphi)}{2}\left(1+\alpha_{FS}\frac{\sigma_{\perp\max}(\theta,\varphi)}{S_{Yc}}\right)\right]=\left(\frac{\tau_c}{G}\right)(2N)^{b_\gamma}+\gamma_c(2N)^{c_\gamma} \tag{8}$$

$$\frac{\frac{1}{2}\Delta\sigma_\perp(\theta,90°)}{S_F(N)}+\frac{\sigma_{\perp\max}(\theta,90°)-\frac{1}{2}\Delta\sigma_\perp(\theta,90°)}{S_U}=1 \tag{9}$$

$$\max_{\theta,\varphi}\left[\sigma_{\perp\max}(\theta,\varphi)\frac{\Delta\varepsilon_\perp(\theta,\varphi)}{2}\right]=\left(\frac{{\sigma_c}^2}{E}\right)(2N)^{2b}+\sigma_c\varepsilon_c(2N)^{b+c} \tag{10}$$

Findley's shear model, Eq. (7), assumed fatigue damage being mainly caused by the combination of the peak normal stress ($\sigma_{\perp max}$) perpendicular to the critical plane with the amplitude of the shear stress ($\Delta\tau/2$). Fatemi-Socie, Eq. (8), is another shear model which assumes that, instead of stress, the shear strain amplitude ($\Delta\gamma/2$) is the fatigue driving force along with the peak perpendicular stress. Also, a multiplicative parameter is used instead of the additive one to correct for a wrong fatigue damage prediction that would happen under small non-damaging shear stresses and/or strain ranges.

For tensile sensitive materials, Goodman's alternate-mean equation commonly used in uniaxial fatigue can be adapted to a Generalized Goodman tensile model, Eq. (9), considering the alternate and mean of the plane's perpendicular stress ($\sigma_\perp$). Another recommended model is the Smith-Watson-Topper's (SWT) critical-plane tensile model, Eq. (10), also an adaptation from a uniaxial low-cycle fatigue model, considering in this version the peak normal stress and normal strain amplitude, both perpendicular to the critical plane, as the main cause of damage.

2.6 **Curve Fitting**

For both tensile-compression and torsional life prediction curves, the experimental data was fitted by Coffin-Manson's εN curve and its shear version γN using the Levenberg-Marquardt algorithm. In the εN curve-fitting, the given data is: Young Modulus, vector of applied strain amplitudes (ε_a) and corresponding vector of resulting number of cycles to failure (N). The working variables are: σ_c, ε_c, b and c. Similarly, in the γN curve-fitting, the given data is the Shear Modulus and the vectors γ_a and N, with the working variables as τ_c, γ_c, b_γ and c_γ.

To fit a curve that is physically admissible, a proper choice of boundary values for the working variables is necessary. In the present work, they were chosen to encompass the possible values from a variety of experimental data and estimative propositions listed on Castro et al. The mentioned data indicates that most metallic structural alloys have their elastic and plastic exponents in the range of $-0.2 < b < -0.05$ and $-0.9 < c < -0.3$, respectively. For that reason, the shown intervals were chosen as the exponent boundaries. Lagoda et al. states that it is of common practice among authors to assume parallelism between εN and γN equations, considering $b=b_\gamma$ and $c=c_\gamma$.

Through the proposed estimates and experimental data presented in Castro et al, a reasonable boundary for the elastic and plastic coefficients is $S_u < \sigma_c < 2S_u$ and $\varepsilon_y < \varepsilon_c < \varepsilon_u$, where S_u is the ultimate strength and ε_y and ε_u are the deformation in the yield and ultimate strengths, respectively. For the shear coefficients, the upper boundaries were repeated and the lower boundaries were divided by 2.

2.7 **Comparison Procedures**

The εN and γN curve comparison is a good way to determine if the material is shear or tensile sensitive. It is necessary, though, to transform the γN curve into an equivalent εN for a plot comparison, in which the curve that appears lower on the plot is the one where the material fails under lower equivalent strain variations.

In the present work, 2 equivalent strain curves are calculated from the γN one, using the von Mises and Tresca Failure Criteria, as shown in Eqs. (11) and (12) respectively:

$$(\varepsilon N)_{MISES}=\frac{\sqrt{3}}{2(1+\bar{\nu})}(\gamma N) \tag{11}$$

$$(\varepsilon N)_{TRESCA}=\frac{1}{(1+\bar{\nu})}(\gamma N) \tag{12}$$

where $\bar{\nu}$ is the effective Poisson ratio, a value in-between the elastic and plastic Poisson ratios ($\nu \leq \bar{\nu} \leq 0.5$). Since the experiments in the present work where conducted with high strain values, $\bar{\nu}$ is assumed to be equal to the plastic Poisson ratio, reducing Eqs. (11-12) to:

$$(\varepsilon N)_{MISES} = \frac{1}{\sqrt{3}}(\gamma N) \tag{13}$$

$$(\varepsilon N)_{TRESCA} = \frac{2}{3}(\gamma N) \tag{14}$$

3. RESULTS

The tensile-test mechanical properties for each material are listed in Table 2. For the εN curve fitting, data from Lima et al.'s work was also used along with new data acquired in the present work. Both εN curves are shown in Figure 6 and Eqs. (15-16). For the γN curve fitting, ten (φ_a, N) points were measured for each material and converted to (γ_a, N) points, as shown in Figure 7, resulting in Eqs. (17-18). All angular displacements and their corresponding number of cycles are listed in Table 3. Figure 8 shows the comparison between the fitted εN curves and the ones obtained from the shear data using von Mises and Tresca criteria.

$$SAE\ 1020\ Steel\text{:}\ \varepsilon_a = \left(\frac{893.9}{E}\right)(2N)^{-0.099} + 0.368(2N)^{-0.515} \tag{15}$$

$$6351 - T6\ Aluminum\text{:}\ \varepsilon_a = \left(\frac{555.7}{E}\right)(2N)^{-0.092} + 0.268(2N)^{-0.682} \tag{16}$$

$$SAE\ 1020\ Steel\text{:}\ \gamma_a = \left(\frac{824.2}{G}\right)(2N)^{-0.112} + 0.336(2N)^{-0.476} \tag{17}$$

$$6351 - T6\ Aluminum\text{:}\ \gamma_a = \left(\frac{548.1}{G}\right)(2N)^{-0.099} + 0.458(2N)^{-0.590} \tag{18}$$

Table 2. Mechanical properties for SAE 1020 and 6351-T6 Al

Property	SAE 1020 Steel	6351-T6 Aluminum
S_y	558 MPa	324 MPa
S_u	599 MPa	352 MPa
ν	0.29	0.32
E	194.4 GPa	68.2 GPa
G	75.35 GPa	25.83 GPa
Area reduction (AR)	40%	57%
ε_y	0.00287	0.00475
ε_u	0.616	0.844

Table 3. Angular displacements and their corresponding number of cycles up to failure for SAE 1020 and 6351-T6 Al

SAE 1020 Steel		6351-T6 Aluminum	
Angular displacement (φ_a)	Number of cycles up to failure (N)	Angular displacement (φ_a)	Number of cycles up to failure (N)
8	1038	7	763
7	2230	6	874
6	2889	5	1780
5	5190	5	2030
4	10260	4.5	2525
3.8	11837	4.2	6851
3.8	10839	4	7428
3.5	17507	4	6440
3.5	18747	3.7	8819
3	28664	3.5	18337

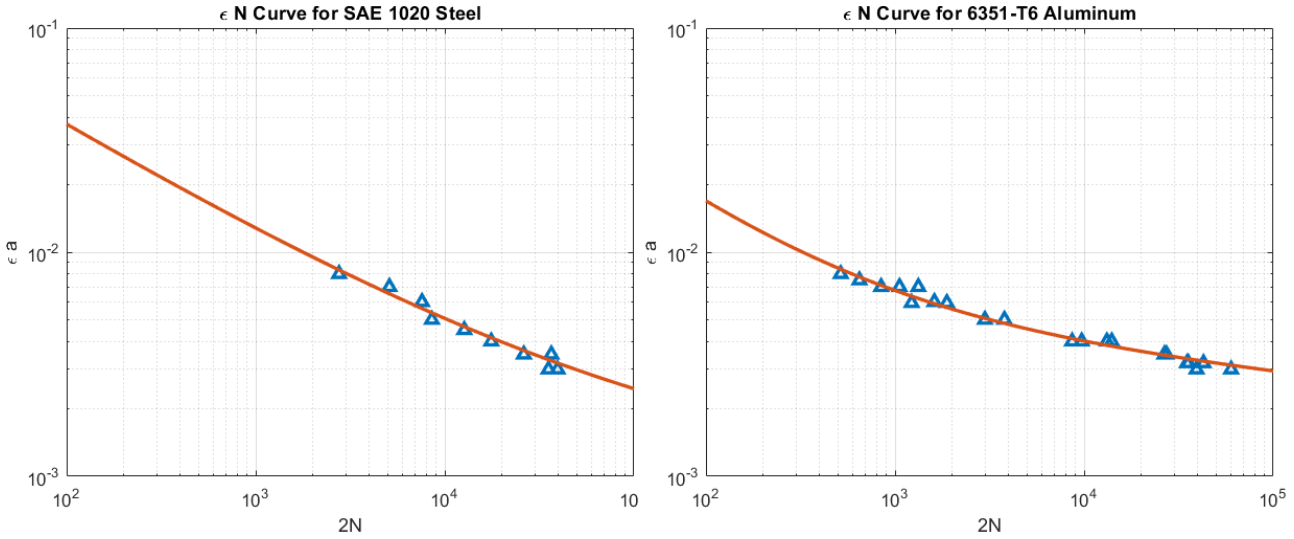

Figure 6. SAE 1020 and 6351-T6 Al εN curves

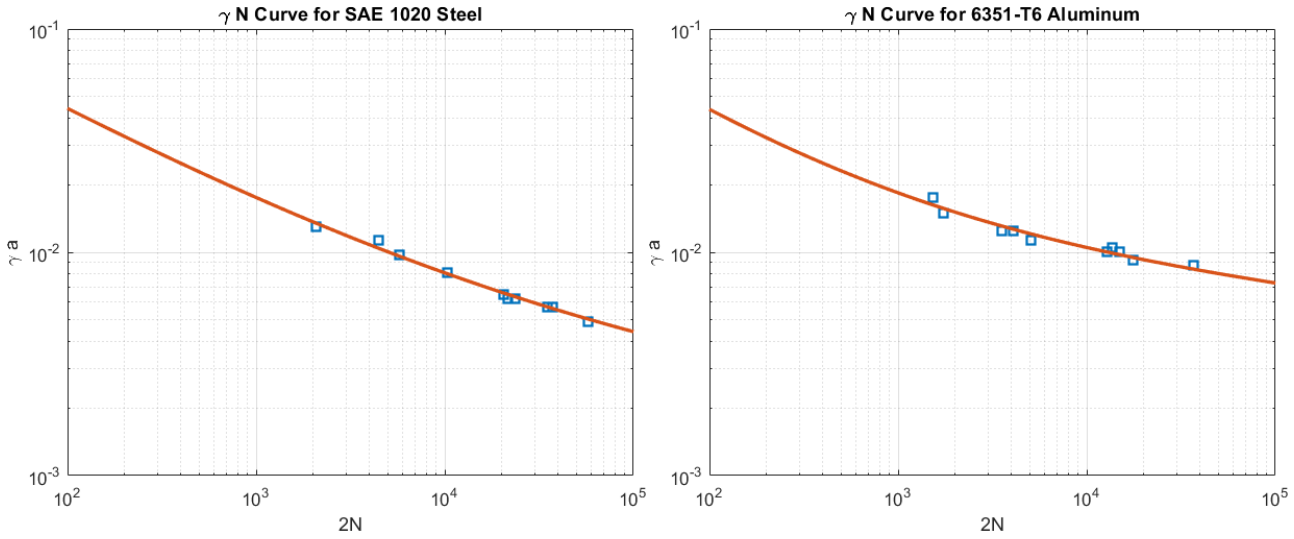

Figure 7. SAE 1020 and 6351-T6 Al γN curves.

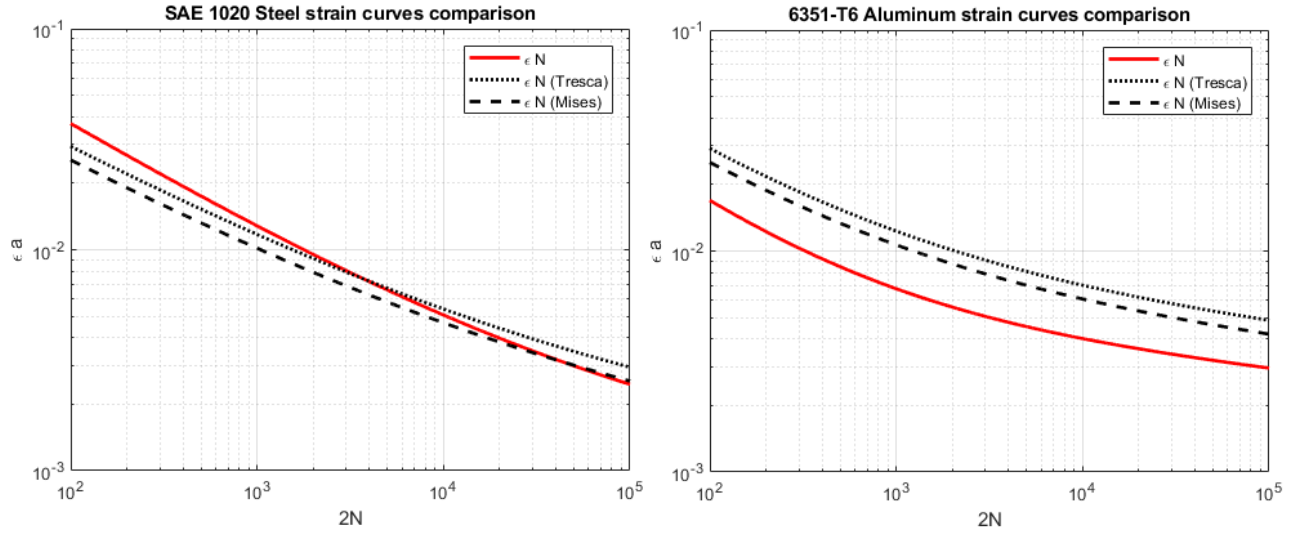

Figure 8. Comparison of εN curves with $(\varepsilon N)_{\mathbf{Mises}}$ and $(\varepsilon N)_{\mathbf{Tresca}}$ equivalent curves for SAE 1020 and 6351-T6 Al

For the 6351-T6 aluminum alloy (Fig. 8 on the right), since the εN curve was lower than the von Mises and Tresca equivalent ones obtained from shear data, it can be concluded that it is more sensitive to tensile deformations and, therefore, models such as SWT and Generalized Goodman are recommended for its fatigue damage calculation.

SAE 1020 steel, on the other hand, had mixed results. As seen in Fig. 8 (left), under low cycle fatigue its εN curve was higher than the von Mises and Tresca equivalent ones obtained from shear data. Therefore, shear-sensitive models such as Findley and Fatemi-Socie are recommended for its low cycle fatigue calculations. Note however that, under high cycle fatigue, this trend tends to reverse, with tensile damage becoming the major damage mechanism, as the εN curve drops below the equivalent ones. In summary, the studied data indicates that this steel is shear-sensitive under low-cycle fatigue, and tensile-sensitive for longer lives.

4. CONCLUSION

In this work, low-cycle fatigue properties were measured for SAE 1020 steel and 6351-T6 aluminum alloys. A simplified method was proposed to semi-empirically estimate the low-cycle fatigue properties under torsional constraints. This method was used to measure the shear (γN) low-cycle fatigue properties for each material. The Levenberg-Marquardt algorithm was used to fit the Coffin-Manson curve and its shear equivalent for each material. Using both sets of data, each material was characterized as either shear or tensile sensitive, and the most appropriate multiaxial critical-plane fatigue damage models were recommended accordingly.

5. REFERENCES

Castro, J.T.P. and Meggiolaro, M.A., 2016. “Fatigue design techniques” (in 3 volumes). CreateSpace, Scotts Valley, CA, USA.

Standard, A.S.T.M., 2004. E606-92,". Standard Practice for Strain-Controlled Fatigue Testing,” Annual Book of ASTM Standards, 3.

Lagoda, T., Kulesa, A., Kurek, A. and Koziarska, J., 2018. Correlation of Uniaxial Cyclic Torsion and Tension-Compression for Low-Cycle Fatigue. Materials Science, 53(4), pp.522-531.

Handbook, A.S.M., 1990. Vol. 1. Properties and Selection: Irons, Steels, and High Performance Alloys. ASM international, 1.

Handbook, A.S.M., 1990. Vol. 2. Properties and Selection: Nonferrous Alloys and Special-Purpose Materials. ASM international, 1.

Standard, A.S.T.M., 2001. E8–99. "Standard Test Methods for Tension Testing of Metallic Materials." Annual book of ASTM standards.

Lima, G.W., 2018. Determinação Experimental do Limite de Fadiga de uma Liga de Alumínio por Termografia (undergraduate thesis)

Standard, A. S. T. M. "E2207-02." Standard practice for strain-controlled axial-torsional testing with thin walled tube specimens. Annual Book of ASTM Standards 3 (2007): 1297-1304.

Gere, James M., and S. P. Timoshenko. "Mechanics of Materials 2e." Brooks/Cole Engineering 198, no. 4 (1984).

6. RESPONSIBILITY NOTICE

The authors are the only responsible for the printed material included in this paper.